Nonreciprocal flexural dynamics of Dzyaloshinskii domain walls

R. Soucaille,[1,2,*] F. Garcia-Sanchez,[1,3] J.-V. Kim,[1] T. Devolder,[1] and J.-P. Adam[1,†]

[1]*Centre de Nanosciences et de Nanotechnologies, CNRS, Université Paris-Sud, Université Paris-Saclay, 91405 Orsay cedex, France*

[2]*School of Physics, University of Exeter, Stocker Road, Exeter EX4 4QL, United Kingdom*

[3]*Istituto Nazionale di Ricerca Metrologica, Strada delle Cacce 91, 10135 Torino, Italy*

(Received 11 February 2018; revised manuscript received 2 July 2018; published 24 August 2018; corrected 7 September 2018)

We revisit the description of ferromagnetic domain wall dynamics through an extended one-dimensional model by allowing flexural distortions of the wall during its motion. This is taken into account by allowing the domain wall center and internal angle to be functions of position in the direction parallel to the wall. In the limit of small applied fields, this model accounts for the nonreciprocity in the propagation of wall modes and their stability in the presence of the Dzyaloshinskii-Moriya interaction and in-plane magnetic field.

DOI: 10.1103/PhysRevB.98.054426

I. INTRODUCTION

The dynamics of ferromagnet domain walls encompasses a wide range of nonlinear phenomena. A prime example is Walker breakdown, which represents the transition between the steady state motion of a wall under applied fields or currents and the precessional regime in which the wall motion is oscillatory. Despite the complexity of the magnetic interactions and dynamics governing individual moments in a given material system, many of the salient features of domain wall motion can be captured by a one-dimensional model in which the wall center, $u(t)$, and internal wall angle, $\phi(t)$, are the only variables that describe the dynamics [1,2]. For example, the magnetic field dependence of the wall velocity predicted by the model has been observed in in-plane magnetized wires [3].

Despite the utility of the one-dimensional model, a large number of experimental observations cannot be accounted for by this description. For example, magnetic disorder can prevent the Walker transition from being attained or even identified clearly [4], and leads to a low-field creep regime where thermally activated processes are dominant [5]. Beyond the creep regime, other deviations from the one-dimensional picture have been observed in perpendicularly magnetized ultrathin ferromagnets. Instabilities in the wall structure lead to plateaus in the velocity versus field curves [6,7], which are largely driven by incoherent magnetization precession at the wall center [8]. Due to this incoherent precession, Néel or Bloch lines are created within and move along these domain walls, leading to periodic annihilation events resulting in spin wave bursts [9]. A number of previous works have addressed such shortcomings in different ways. For the dynamics of vortex walls in in-plane magnetized systems, an extended model has been developed that also accounts for the internal dynamics of the vortex in addition to the usual wall variables [10,11]. This approach is based on the method of collective coordinates, which provides a framework to incorporate internal degrees of freedom (such as spin waves) into the dynamics of the underlying spin texture [12–14]. Other work has sought to account for flexural modes of the domain wall, which can be excited during propagation and can lead to clear deviations from the one-dimensional behavior [15]. Evidence of wall flexing has been obtained in low-moment ferromagnets [16].

In ultrathin ferromagnets, the proximity of a strong spin-orbit coupling material can give rise to an additional chiral interaction of the Dzyaloshinskii-Moriya form [17–19]. Besides favoring Néel-type domain walls at equilibrium [20–25], this interfacial Dzyaloshinskii-Moriya interaction (iDMI) results in the asymmetric nucleation [26] and growth of magnetic domains in perpendicularly magnetized ferromagnetic films under in-plane applied fields, where domain wall propagation is affected in the creep, steady state, and precessional regimes [21,27–38]. With respect to internal modes, it has also been shown that spin wave channeling by domain walls can acquire a nonreciprocal character [39,40], which is similar to behavior seen for magnetostatic spin wave modes induced by dipolar effects [41]. Some theoretical work has been undertaken to explore how the iDMI affects the wall motion in the creep regime [42], but there remain open questions on its role in the dynamics of flexural modes.

Here, we introduce an intermediate model between a full micromagnetic description of a domain wall and the 1D model [21]. We explicitly allow for a nonuniform propagation of the domain wall, where the spatial dependence of the wall center is taken into account. This model allows us to have a more complete description of the domain wall dynamics. We will focus on the bending motion of a straight domain wall with the iDMI and in-plane field. To describe the dynamics of the domain wall, especially at long wavelengths, we model the evolution of the domain wall dynamics in a system with perpendicular magnetic anisotropy and in the presence of the iDMI. We also examine the effect of a small in-plane magnetic field and pinning potentials.

The article is organized as follows. In Sec. II, we compute the dynamics of the domain wall via a Lagrangian description

*remy.soucaille@gmail.com

†jean-paul.adam@u-psud.fr

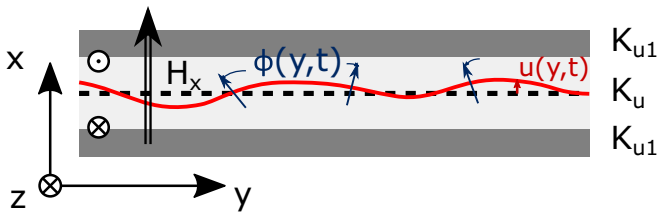

FIG. 1. Geometry for the domain wall dynamics. The domain wall is set at the center (dotted line). An anisotropy well where $K_u < K_{u,1}$ is used to model the effect of the pinning. The two functions $\phi(y,t)$ and $u(y,t)$ parametrize respectively the in-plane angle and the domain wall position. The red line is a schematic of the domain wall position during an excitation.

of the magnetic texture. Our model is a direct extension of the 1D model where the magnetization is supposed rigid. In Sec. III, we compare the obtained result for the flexural motion with micromagnetic simulations. In Sec. IV, we discuss in more detail the nonreciprocity of the flexural modes. Some concluding remarks are provided in Sec. V.

II. DOMAIN WALL ENERGY AND DYNAMICS

We describe the energy and dynamics of a magnetic domain wall in an ultrathin film in this section. Within the micromagnetic description, the magnetization unit vector $\mathbf{m} = \mathbf{M}/M_s$ can be described by the two spherical angles θ and ϕ,

$$\mathbf{m}(\theta,\phi) = (\sin\theta\cos\phi, \sin\theta\sin\phi, \cos\theta). \tag{1}$$

We consider a domain wall running along the y direction that separates two magnetic domains along the x direction. The magnetization within each domain is taken to point along the z direction, perpendicular to the film plane. A schematic illustration of this geometry is given in Fig. 1.

We assume that the component of the magnetization perpendicular to the plane, parametrized by the polar angle θ, can be described by the usual profile,

$$\theta(x,y,t) = 2\tan^{-1}\left[\exp\left(\frac{x-u(y,t)}{\Delta}\right)\right], \tag{2}$$

where $u(y,t)$ represents the domain wall center and $\Delta = \sqrt{A/K_{\text{eff}}}$ is the domain wall width, which remains constant. A is the exchange constant and K_{eff} is the perpendicular anisotropy constant. Both θ and ϕ are assumed to be uniform across the film thickness along z. We also assume that ϕ is uniform along the x direction, $\phi = \phi(y,t)$, and that the domain wall remains close to a straight configuration ($||\partial u/\partial y|| \ll 1$).

We now describe the different contributions to the magnetic energy densities with this ansatz. The effective perpendicular uniaxial anisotropy is given by

$$\mathcal{E}_{\text{anis}} = K_{\text{eff}} d \int \sin^2\theta\, dx = \frac{1}{2}\sigma_0 d, \tag{3}$$

where d is the film thickness and $\sigma_0 = 4\sqrt{AK_{\text{eff}}}$ is the Bloch wall energy. This energy is independent of the displacement u and the angle ϕ. The exchange interaction energy density is given by

$$\begin{aligned}\mathcal{E}_{\text{ex}} &= Ad\int[(\nabla\theta)^2 + \sin^2\theta(\nabla\phi)^2]dx \\ &= \frac{1}{2}\sigma_0 d\left[1 + \left(\frac{\partial u}{\partial y}\right)^2 + \Delta^2\left(\frac{\partial\phi}{\partial y}\right)^2\right].\end{aligned} \tag{4}$$

The (positive) squared derivative terms are a reminder that the exchange energy favors a uniform configuration along the transverse (i.e., y) direction. The sum of these two terms give the usual domain wall energy, σ_0, with additional contributions to the wall elastic energy, proportional to $(\partial_y u)^2$ and $(\partial_y\phi)^2$, which arise from small deformations from the straight wall profile.

In perpendicularly magnetized films described by these two magnetic energies only, domain walls are of the Bloch type which minimize volume dipolar charges. Deviations from this profile can appear when other interactions are present.

First, proximity of a strong spin-orbit coupling material to the ferromagnetic film induces an iDMI, which can be described by [21,43]

$$\begin{aligned}\mathcal{E}_{\text{D}} &= Dd\int[m_z(\nabla\cdot\mathbf{m}) - (\mathbf{m}\cdot\nabla)m_z]dx \\ &= -\pi Dd\left(\cos\phi - \frac{\partial u}{\partial y}\sin\phi\right),\end{aligned} \tag{5}$$

where D is the iDMI constant expressed in J/m^2. One can rewrite this equation as a function of $\phi + \tan^{-1}(\partial u/\partial y)$ and the length of the domain wall which shows that the iDMI effective field [44] is always normal to the domain wall.

Second, applied magnetic fields can also modify the wall profile. The effect of a magnetic field $\mathbf{H}$ can be separated into two parts, an in-plane ($//$) and an out-of-plane ($\perp$) component. The out-of-plane component results in domain wall displacement and contributes to the total energy density through the Zeeman interaction as

$$\mathcal{E}_{Z,\perp} = -2\mu_0 M_s H_z u d. \tag{6}$$

In contrast, the in-plane component leads to changes in the internal structure ϕ of the domain wall. In the limit of a small applied in-plane magnetic field, $\sqrt{H_x^2 + H_y^2} \ll H_K$, where $H_K = 2K_{\text{eff}}/\mu_0 M_s$ is the effective anisotropy field, the associated Zeeman term is

$$\mathcal{E}_{Z,//} = -\pi\mu_0 M_s \Delta d(H_x\cos\phi - H_y\sin\phi). \tag{7}$$

Note that as compared to the one-dimensional model [44] we have an additional term proportional to $\partial_y u$ in the iDMI energy, which is absent in the Zeeman energy. While part of the iDMI energy can still be assimilated to an effective magnetic field along the x direction, we note that the y component of the effective field is linked to gradients in the domain wall displacement u, $\partial_y u$. This result may provide a theoretical basis for asymmetric domain growth that has been observed experimentally in the presence of in-plane fields [27,29,32,34,42,45].

We approximate the dipolar interaction with a transverse anisotropy term, $\mathcal{E}_\perp$. We assume that the domain wall profile varies slowly compared to the domain wall width and consider

flexural modes in the long-wavelength limit, $k\Delta \ll 1$. Under this approximation, we can write [46]

$$\mathcal{E}_\perp = 2K_\perp \Delta d \cos\left[\phi + \tan^{-1}\left(\frac{\partial u}{\partial y}\right)\right]^2, \tag{8}$$

where $K_\perp = (\ln 2)\mu_0 M_s^2 d/\pi\Delta$ accounts for the difference in dipolar energy between the Néel and Bloch wall profiles [47]. We note that the dipolar interaction, like the iDMI, leads to a coupling between the internal angle ϕ and deformations in the wall, $\partial_y u$. The dipolar interaction favors the Bloch profile, where the magnetization at the wall center is tangent to the domain wall, while the interfacial iDMI favors the Néel profile, where the magnetization at the wall center is normal to the domain wall. Finally, domain wall pinning due to material inhomogeneities needs to be taken into account for realistic systems. This can be introduced by assuming a quadratic potential well of the form

$$\mathcal{E}_{\text{pin}} \approx \tfrac{1}{2}\kappa u^2 d, \tag{9}$$

where κ characterizes the strength of the pinning potential. A quadratic well will be valid only close to the pinning line. For larger displacements of the domain wall we might consider the real pinning landscape. This pinning landscape corresponds to the convolution between the function describing the change in anisotropy and the hyperbolic form of the Bloch domain wall profile. For a line defect the pinning potential is the same as in the 1D domain wall framework [48] where the pinning potential of a line defect located at u_0 is

$$\mathcal{E}_{\text{pin,line}} = V_0 \text{sech}^2[(u-u_0)/\Delta]. \tag{10}$$

In the case of a point defect, we should use a similar function for the pinning landscape and replace the distance $u - u_0$ by the distance between the pinning center and the domain wall coordinate. In this case a strong attractive pinning center will tend to fix the domain wall at the pinning center.

For systems with uniform properties along the y axis, such as the line anisotropy defect shown in Fig. 1, we can assume that the equilibrium domain wall profile is also uniform along this direction. As such, $\phi(y) = \phi_0$ and all spatial derivatives in the domain wall position are vanishing, $\partial u/\partial y = 0$. The equilibrium angle ϕ_0 can be determined by minimizing the total energy. In the case where the in-plane field is applied along the x direction, ϕ_0 is given by [47]

$$\phi_0 = \begin{cases} \pi, & \mu_0\pi M_s H_x < \pi D/\Delta - 2K_\perp, \\ 0, & \mu_0\pi M_s H_x > \pi D/\Delta + 2K_\perp, \\ 2\tan^{-1}\left[\sqrt{\frac{2K_\perp+\pi D/\Delta+\mu_0\pi M_s H_x}{2K_\perp-\pi D/\Delta-\mu_0\pi M_s H_x}}\right], & \text{otherwise.} \end{cases} \tag{11}$$

Depending on the in-plane field the domain wall structure transforms from a right-handed Néel wall to a left-handed Néel passing through a mixed Néel/Bloch wall.

We now discuss the dynamics of the domain wall as an elastic line using Lagrangian formalism to derive the equations of motion of the domain wall. For spin dynamics, the Lagrangian density for the spherical angles θ and ϕ can be written as [49,50]

$$\mathcal{L} = \frac{M_s d}{\gamma}\int \dot{\phi}(1-\cos\theta)\,dx - \mathcal{E}[\theta,\phi], \tag{12}$$

where the first term on the right-hand side is the Berry phase term and $\mathcal{E}(\theta,\phi)$ is the total energy density of the domain wall, which is the sum of the different contributions given in Eqs. (3) to (8). By using the domain wall ansatz in Eq. (2), integrating over x, and neglecting terms which are not relevant for the dynamics of the system, we find

$$\mathcal{L} = -2\frac{M_s d}{\gamma}\dot{\phi}u - \mathcal{E}[u,\phi]. \tag{13}$$

Gilbert damping can be accounted for through the dissipation function

$$\mathcal{W}_{\text{G}} = \alpha\frac{M_s d}{2\gamma}\int(\dot{\theta}^2 + \dot{\phi}^2\sin^2\theta)dx, \tag{14}$$

which, with the same ansatz, leads to the density

$$\mathcal{W}_{\text{G}} = \frac{\alpha M_s \Delta d}{\gamma}\left(\frac{\dot{u}^2}{\Delta^2} + \dot{\phi}^2\right). \tag{15}$$

The equations of motion correspond to the usual Euler-Lagrange equations,

$$\frac{d}{dt}\frac{\partial\mathcal{L}}{\partial(\partial_t u)} + \frac{d}{dy}\frac{\partial\mathcal{L}}{\partial(\partial_y u)} - \frac{\partial\mathcal{L}}{\partial u} + \frac{\partial\mathcal{W}_{\text{G}}}{\partial(\partial_t u)} = 0, \tag{16}$$

$$\frac{d}{dt}\frac{\partial\mathcal{L}}{\partial(\partial_t \phi)} + \frac{d}{dy}\frac{\partial\mathcal{L}}{\partial(\partial_y \phi)} - \frac{\partial\mathcal{L}}{\partial \phi} + \frac{\partial\mathcal{W}_{\text{G}}}{\partial(\partial_t \phi)} = 0. \tag{17}$$

Explicitly, this leads to the set of coupled nonlinear differential equations,

$$\begin{aligned} &\frac{2M_s}{\gamma}\frac{\partial\phi}{\partial t} + \frac{M_s\alpha}{\gamma\Delta}\frac{\partial u}{\partial t} - \sigma_0\frac{\partial^2 u}{\partial y^2} - \pi D\frac{\partial\phi}{\partial y}\cos\phi \\ &- 2\mu_0 M_s\pi H_z + \kappa u - K_\perp\Delta\left[\frac{\partial\chi}{\partial y}\sin 2(\chi+\phi)\sin 2\chi\right. \\ &\left. - 2\cos 2(\chi+\phi)\left(\frac{\partial\phi}{\partial y} + \frac{\partial\chi}{\partial y}\right)\cos^2\chi\right] = 0, \end{aligned} \tag{18}$$

$$\begin{aligned} &-\frac{2M_s}{\gamma}\frac{\partial u}{\partial t} + \frac{M_s\alpha}{\gamma}\Delta\frac{\partial\phi}{\partial t} - 4A\Delta\frac{\partial^2\phi}{\partial y^2} \\ &+ \pi D\left(\frac{\partial u}{\partial y}\cos\phi + \sin\phi\right) - K_\perp\Delta\sin(2\chi+2\phi) \\ &+ \mu_0 M_s\pi\Delta(H_x\sin\phi - H_y\cos\phi) = 0, \end{aligned} \tag{19}$$

where $\chi \equiv \tan^{-1}(\partial u/\partial y)$. Note that we recover the usual one-dimensional domain wall model [21] when the spatial derivatives in u and ϕ are set to zero.

III. DISPERSION RELATION OF THE FLEXURAL MODE

In this section we focus on the dispersion relation for the flexural dynamics of the domain wall derived from the Lagrangian formalism in the previous section. We limit our study to the case where the slope of the wall is small, $\partial u/\partial y \ll 1$, for large wavelengths, $k\Delta \ll 1$, and for small applied in-plane fields along the normal to the domain wall, $H_{//} = H_x \ll H_{\text{K}_{\text{eff}}}$. A first-order series expansion on the set of two coupled differential equations is done over $u(y,t)$ and $\phi(y,t)$ around $\phi = \phi_0$ and $u = 0$, where ϕ_0 is the equilibrium angle of the magnetization. We then look for the propagating solutions of theses equations to get the dispersion relation $\omega(k)$,

which is found to be

$$\omega(k) = \Omega_{\mathrm{NR}} + \sqrt{\Omega_u \Omega_\phi}, \tag{20}$$

where Ω_{NR} is linear with respect to the wave vector and is responsible for nonreciprocal propagation,

$$\Omega_{\mathrm{NR}} = \omega_{\mathrm{D},k} \cos\phi_0 - k\Delta\omega_\perp \cos 2\phi_0. \tag{21}$$

Ω_u describes the stiffness of the domain wall position,

$$\Omega_u = \omega_k + \omega_{\mathrm{pin}} - (k\Delta)^2 \omega_\perp \cos 2\phi_0, \tag{22}$$

and Ω_ϕ describes the stiffness of the angle ϕ of the magnetization,

$$\Omega_\phi = \omega_k + \frac{\omega_{\mathrm{D},k}}{k\Delta} \cos\phi_0 + \omega_{H,x} \cos\phi_0 - \omega_\perp \cos 2\phi_0. \tag{23}$$

The angular frequencies in Eqs. (21) to (23) are given by [40]

$$\omega_k = 2\frac{\gamma A}{M_s} k^2, \tag{24}$$

$$\omega_{\mathrm{D},k} = \frac{\pi}{2}\frac{\gamma D}{M_s} k, \tag{25}$$

$$\omega_\perp = \frac{\gamma K_\perp}{M_s}, \tag{26}$$

$$\omega_{H,x} = \frac{\pi}{2}\gamma\mu_0 H_x, \tag{27}$$

$$\omega_{\mathrm{pin}} = \frac{1}{2}\frac{\gamma\Delta}{M_s}\kappa. \tag{28}$$

We note that this description provides a more accurate treatment of the dipolar interaction at long wavelengths in comparison to previous work [40,51,52], since we take into account fluctuations in the wall position through the term $\partial_y u$.

The variation of the flexural mode frequency with applied in-plane field, H_x, and the wave vector, k, is presented in Fig. 2. In this figure the saturation magnetization is taken to be $M_s = 788$ kA/m, the exchange stiffness $A = 22.5$ pJ/m, the uniaxial anisotropy $K_0 = 641.5$ kJ/m^3, and the iDMI $D = 0.28$ mJ/m^2. These values represent the material system W(3 nm)/CoFeB(1 nm)/MgO, as discussed in Ref. [35]. The dispersion relation allows us to identify instabilities in the straight domain wall configuration assumed as the equilibrium profile. Instabilities occur when the mode frequency vanishes, which typically corresponds to a change in the equilibrium state. We note that the uniform mode, $k = 0$, which corresponds to the uniform displacement of the domain wall, is not necessarily the eigenmode with the lowest energy. This can be seen in Fig. 2, where there are two field intervals over which the straight domain wall is unstable. Similarly to the case where the iDMI is strong enough to create maze domain patterns [40], this instability occurs for one propagation direction of the flexural mode.

Unlike this case, here the domain wall energy is still positive and the sign of the wave vector which leads to negative frequency depends on the chirality of the domain wall and on D. This instability is shown in Fig. 2, where the frequency reaches negative values for wave vectors between 0 and 10 μm^{-1} at around -50 mT and for $-5\ \mu\mathrm{m}^{-1} < k < -1\ \mu\mathrm{m}^{-1}$ at -20 mT. For an applied in-plane field value close to the field value corresponding to the iDMI strength a straight wall is stable. This result is surprising since one expects faceting

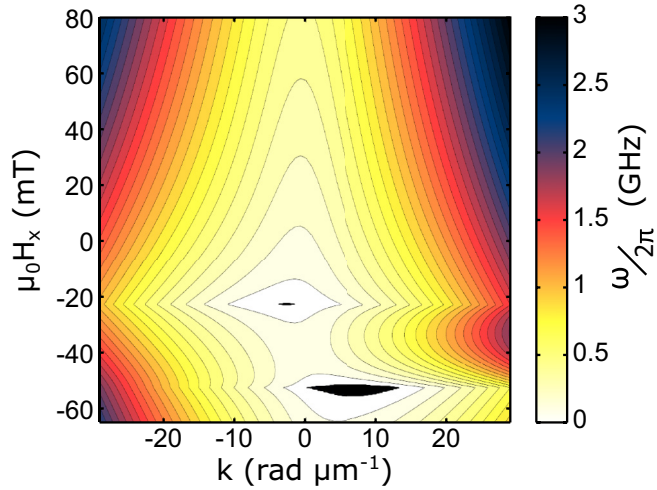

FIG. 2. Dispersion relation of the flexural motion of the domain wall with respect to the in-plane field $\mu_0 H_x$ normal to the domain wall and the wave vector k_y which propagates along the domain wall [from Eq. (20)]. The wall is pinned in an anisotropy well with a width of 80 nm. Contour lines are separated by 100 MHz and the black areas close to -20 mT and -50 mT represent the $(\mu_0 H_x, k_y)$ space range in which the frequencies are negative, indicating straight domain wall instabilities.

of the wall when the in-plane field compensates the iDMI field [37,42]. We do not find such an instability here. This is linked to the initial state that we have considered, where ϕ_0 is constant in the initial configuration whereas for a curved domain wall ϕ_0 can vary along the domain wall. The two sides of facets have opposite slope $(\partial u/\partial y)$ and opposite angle ϕ. To create facets the angle ϕ needs to go continuously from positive to negative value. For this, the domain wall needs to overcome an energy barrier which is linked to the dipolar interaction: a straight domain wall configuration is a metastable state. The dipolar energy has two opposite effects: it broadens the region where a straight wall is metastable and it tends to increase the stability of the domain wall in this region by increasing the energy barrier. For example, if we do not consider the dipolar interaction [Eq. (8)] the two regions of instability in Fig. 2 merge into one region which is centered close to the iDMI effective field.

We compared the analytical model with full micromagnetic simulations using MUMAX3 [53]. The simulation consists of a domain wall pinned in an anisotropy well where the uniaxial anisotropy is increased by 10% outside the well. The width of the anisotropy well is taken to be 80 nm. The dynamics are induced by a pulsed magnetic field, with a time dependence given by a sinc function, along the z direction localized at the center of the frame. The cutoff frequency of the pulse is 10 GHz and the region where the pulse is applied is 4×80 nm^2. The simulation geometry is given by a rectangular window with dimensions of 8 μm$\times$125 nm, which is discretized with 2048×64 finite-difference cells. The layer thickness is 1 nm and periodic boundary conditions are applied along the y direction (along the domain wall). The Gilbert damping constant is set to $\alpha = 0.015$. Other micromagnetic parameters are given earlier and are the same as for Fig. 2.

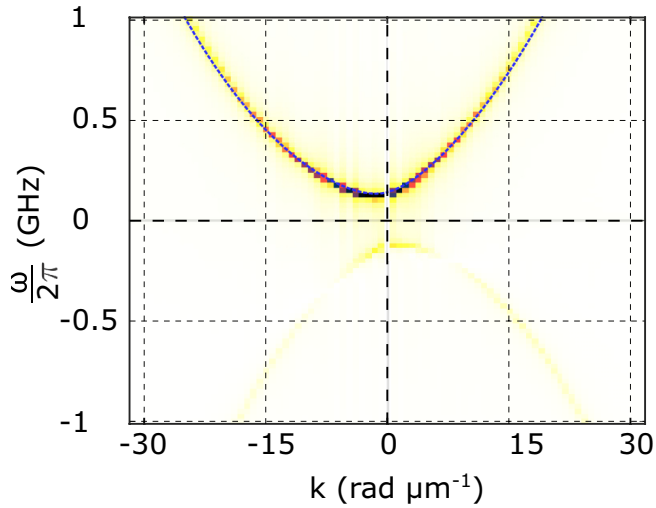

FIG. 3. Detail of the dispersion relation for an applied field $\mu_0 H_x = -10$ mT. It corresponds to the 2D Fourier transform of the function $u + i\Delta\phi$ with respect to the time and the y variable. The blue dotted line corresponds to the dispersion relation given by Eq. (20).

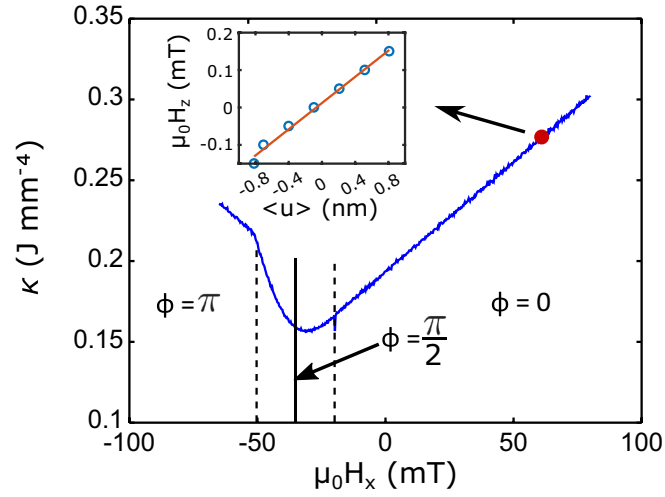

FIG. 4. Variation of the pinning constant κ as a function of the in-plane applied field. The vertical lines delimit the different domain wall configurations for the angle ϕ. The inset shows one example of the fitting between the out-of-plane field with respect to the domain wall position. We deduce the position pinning from this linear fit and from Eq. (29).

In order to compute the full dispersion relation we extract the domain wall position, $u(y,t)$, and the angle of the magnetization at the domain wall center, $\phi(y,t)$. Linear extrapolation is used to obtain values of the displacement smaller than the cell size. The dispersion relation is then computed from a two-dimensional Fourier transform of the complex-valued function $u + i\Delta\phi$, as shown in Fig. 3. It allows us to select the proper branch in the simulated dispersion relation even in the case when the frequency is negative. This is the case when instabilities occur. At this applied field, when the straight wall is unstable, the energy difference between a straight domain wall and the relaxed state is small, and we can still perform micromagnetic simulations starting from a non-fully-relaxed state.

In systems with iDMI the boundary conditions are modified [39,54] which can contribute to pinning. In order to estimate the frequency ω_{pin} [Eq. (27)] linked to the pinning potential acting on the domain wall, we analyze the wall displacement with a small out-of-plane field. We focus on the quadratic pinning potential, Eq. (9), and the Zeeman interaction, Eq. (6). Then, we minimize these two energy terms. The pinning potential is related to the out-of-plane field and the wall position by

$$\kappa = \frac{2\mu_0 M_s H_z}{u}. \tag{29}$$

The pinning potential is then obtained by a linear fit to the positive field branch, as shown in the inset of Fig. 4. The pinning exhibits a strong dependence with respect to the applied field. Its variation is similar to the domain wall width [47]. When the applied field is opposed to the wall chirality the wall width is slightly reduced [47] in our simulation; as the width of the anisotropy well is larger than the wall width the pinning is reduced. From the pinning strength the resonant frequency can be estimated.

A comparison is given in Fig. 5 for the frequency of the uniform $k = 0$ mode, which appears due to the uniform pinning potential as illustrated in Fig. 1. An expression for this frequency is given by

$$\omega_{\text{gap}} = \sqrt{\omega_{\text{pin}}\left(\frac{\pi\gamma D}{2M_s\Delta}\cos\phi_0 - \omega_\perp \cos 2\phi_0 + \omega_{H,x}\cos\phi_0\right)}. \tag{30}$$

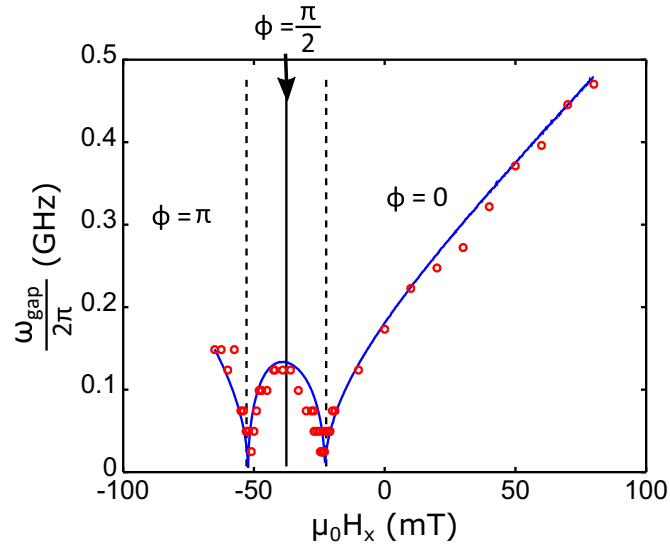

FIG. 5. Influence of the in-plane field on the frequency of the uniform mode, i.e., at $k = 0$. The solid line is derived from the model and circles are the result of micromagnetic simulations. The vertical lines show the different internal angles ϕ of the domain wall at equilibrium.

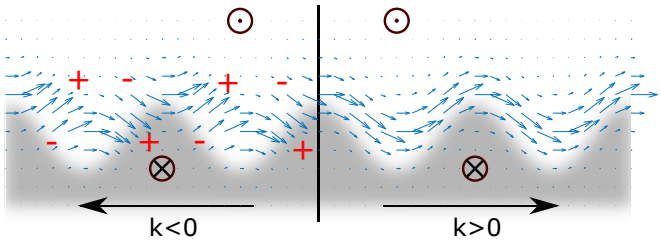

FIG. 6. Illustration of the magnetization state for two opposite propagation directions in the case of a Bloch wall where $\phi_0 = \pi/2$. The "+" and "−" represent the excess of virtual magnetic charges which appear for $k < 0$.

Besides setting the pinning potential to zero (i.e., $K_u = K_{u1}$), the frequency of the uniform mode can also vanish when the applied in-plane field leads to changes in the domain wall profile. This can be seen in Fig. 5 at around $\mu_0 H_x = -20$ mT and -50 mT, where transitions toward the two different chiral Néel domain wall states occur. A very good agreement is obtained between the analytical model and the micromagnetics simulations, both for the critical fields and the uniform mode frequency. The frequency of the uniform mode is obtained from the dispersion relation computed from the micromagnetic simulation. The parameter ω_{pin} is obtained from κ as shown in Fig. 4.

In this section we have seen that an in-plane field allows us to modify the resonant frequency. To properly describe the dynamics of flexural motion of the domain wall in domain walls at relatively low frequencies, i.e., in the sub-GHz range, we have to consider the effect of pinning in the flexural modes.

IV. NONRECIPROCITY OF THE FLEXURAL MODE

In this section we discuss the nonreciprocal behavior of the flexural mode. In the absence of dipolar interactions [40], the frequency difference between two counterpropagating spin waves is proportional to the iDMI constant D. However, as seen in Eq. (21), dipolar interactions also lead to an additional nonreciprocity. While the contribution from the iDMI is periodic with respect to ϕ, the nonreciprocity related to the dipolar interaction is π-periodic [see Eq. (20)] and vanishes when $\phi = \pi/4$. This is related to the fact that the dipolar contribution does not depend on the domain wall chirality but rather on the presence of volume dipolar charges (i.e., whether the wall is of the Bloch or Néel type), whereas the iDMI is sensitive to the domain wall chirality. If we consider a Bloch wall and only the in-plane component of the magnetization, the two counterpropagating waves lead to two different configurations as sketched in Fig. 6.

To have a better picture of this we can consider Eq. (18) where only the exchange interaction and the uniaxial anisotropy are present. In this case the dispersion relation reduces to $\omega = \omega_k$ [see Eq. (24)] and Eq. (18) reads.

$$2\frac{M_s}{\gamma} i\omega_k \phi + k^2 \sigma_0 u = 0. \tag{31}$$

In frequency-momentum space this equation simplifies to $\underline{\phi} = i/\Delta \underline{u}$ where the underline denotes the complex amplitude. We

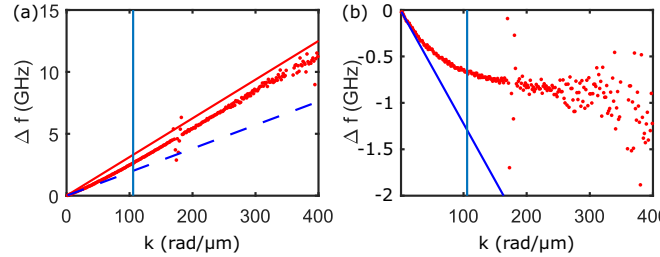

FIG. 7. (a) Evolution of the nonreciprocity with respect to the wave vector. In this simulation the cell size is 0.97 nm. Red dots are results from micromagnetic simulation, the solid red line corresponds to the case where the iDMI is the only source of nonreciprocity, while the dotted blue line corresponds to the approximation to our model where the demagnetizing field is taken locally. The vertical line is for $k = 1/\Delta$. (b) Difference between the simulated nonreciprocity and the contribution of the iDMI.

can see that ϕ and u have a constant $\pi/2$ phase difference. Similarly, the angle χ, which is the angle defined by the tangent of the domain wall, is given by $\underline{\chi} = ik\underline{u}$. For $k = 1/\Delta$ and $\phi_0 = \pm\pi/2$, the in-plane magnetization is tangent to the domain wall. More generally, it leads to two different behaviors depending on the sign of k. For $k > 0$, the angle ϕ and χ are in-phase while for the opposite direction, $k < 0$, they have opposite signs. This will modify the effect of the dipolar interaction for these two cases; when the magnetization tends to be tangent to the domain wall the dipolar energy is reduced. A similar effect occurs for the iDMI. These two interactions (iDMI and dipolar) couple the tilting of the domain wall, χ, with the in-plane magnetization, ϕ, and are at the origin of the nonreciprocity. This is similar to a gyrotropic string which also exhibits a nonreciprocal behavior [55].

In the case of the iDMI energy is smaller than or comparable to the dipolar energy,

$$\pi^2 D \sim 2 \ln 2 \mu_0 M_s^2 d, \tag{32}$$

we cannot neglect the dipolar interaction to describe accurately the nonreciprocity. For $k\Delta \ll 1$, the function $\Delta\omega = \omega(k) - \omega(-k)$ is linear with respect to the wave vector due to both the dipolar and the iDMI contributions. As seen in Fig. 7 the nonreciprocity does not follow the same linear trend for larger wave vectors. When the product $k\Delta$ is close to unity, the dipolar contribution to the nonreciprocity reduces [Fig. 7(b)]. This might be due to the nonlocal component of the dipolar field which is not included in our description. For larger wave vector the slope of the function $\Delta\omega$ seems dominated by the contribution from the iDMI.

In order to have a closer look at the contributions of the different energy terms to the nonreciprocity we have considered the group velocity, defined by $v_g(k) = \partial\omega/\partial k$, as a function of the in-plane magnetic field. We consider only small wave vectors for the group velocity as we assume the $k\Delta \ll 1$ limit. We plot the mean group velocity for two opposite directions (i.e., $[v_g(0^+) + v_g(0^-)]/2$) versus the applied in-plane field in Fig. 8. The two components of the nonreciprocity shown (dotted lines) depend on the in-plane field H_x, which provides a means to modify the nonreciprocity of the domain wall flexural modes. Micromagnetic simulations are in good

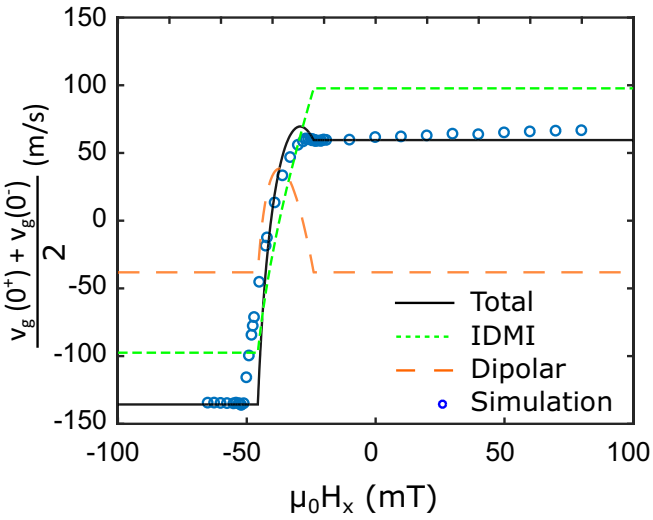

FIG. 8. Evolution of the group velocity for small wave vector with respect to in-plane field $\mu_0 H_x$ along the x axis. Circles are results from micromagnetic simulation; the black line corresponds to the model. The two dotted lines correspond to the iDMI and to the dipolar field contribution to the wall excitation nonreciprocity.

agreement with the model in the long-wavelength limit. As the nonreciprocity is mainly related to the domain wall structure, as soon as the domain wall saturates in one configuration a change in the applied in-plane field no longer modifies the frequency nonreciprocity. Our analytical model allows an accurate description of the nonreciprocity in this case. This long-wavelength regime might be probed in Brillouin light scattering experiments [56] where the wavelength probed is on the order of few hundred nanometers.

For a system where the iDMI interaction is larger (but below $D_{c0} = 4/\pi\sqrt{AK_{\text{eff}}}$), the in-plane magnetic field needed to modify the domain wall orientation can be close to the effective anisotropy field. In this case our model cannot describe the flexural modes quantitatively due to the tilting of the magnetization in the domains and the modification of the domain wall thickness [47]. For large iDMI, the field range where the domain wall is at an intermediate position between Bloch and Néel is suppressed but instabilities of the straight domain wall close to the effective iDMI field are still present and develop toward a specific direction depending on the chirality of the domain wall. The two instability regions merge in a single larger region where the straight wall is unstable and creates facets [37]. The angle of the facets will increase as the magnitude of the iDMI increases. The tilting of the magnetization in the domains will also affect the demagnetizing field and the nonreciprocity in the domain wall modes. We gain insight from Fig. 8 in seeing that the simulated group velocity at $k = 0$ deviates slightly toward positive values. Compared to the nonreciprocity in a Damon-Eshbach configuration, where the magnetization lies in the plane and the spin waves propagate perpendicularly to the magnetization direction, the nonreciprocity is smaller in domain walls. The nonreciprocal part of the dispersion relation is $2Dk\gamma/M_s$ for Damon-Eshbach modes [57] and $\pi Dk\gamma/(2M_s)$ for domain wall modes. In the Damon-Eshbach configuration nonreciprocity can also occur due to the dipolar field, but it depends on the difference between the top and the bottom interface and is proportional to the thickness [58]. The nonreciprocity in the domain wall originates from a different process which is due to the coupling between the wall tilting angle and the magnetization of the domain wall center.

V. CONCLUSION

We have developed an analytical model for domain wall dynamics beyond the one-dimensional model by allowing for inhomogeneous displacements of the domain wall under the influence of a magnetic field. In our model we have supposed that the domain wall structure remains rigid while the domain wall profile is allowed to bend. This description of a flexible domain wall allows for a quantitative analytical description of the flexural mode propagation in the domain wall at long wavelengths. We show that both the interfacial Dzyaloshinskii-Moriya and dipolar interactions contribute to the nonreciprocity of the flexural mode. We have studied the influence of an in-plane field on the domain wall dynamics, which allows the band gap induced by domain wall pinning to be tuned. This field can also induce instabilities in the flexural mode propagation, which take place at the Bloch-Néel transition. This change in the internal wall structure also modifies the direction and the amplitude of the nonreciprocity of the flexural modes.

ACKNOWLEDGMENTS

The authors acknowledge fruitful discussions with Yves Henry and Matthieu Bailleul. This work was partially supported by Agence National de la Recherche (France) under Contract No. ANR-16-CE24-0027 (SWANGATE).

[1] J. C. Slonczewski, J. Appl. Phys. **44**, 1759 (1973).
[2] N. L. Schryer and L. R. Walker, J. Appl. Phys. **45**, 5406 (1974).
[3] G. S. D. Beach, C. Nistor, C. Knutson, M. Tsoi, and J. L. Erskine, Nat. Mater. **4**, 741 (2005).
[4] P. J. Metaxas, J. P. Jamet, A. Mougin, M. Cormier, J. Ferré, V. Baltz, B. Rodmacq, B. Dieny, and R. L. Stamps, Phys. Rev. Lett. **99**, 217208 (2007).
[5] S. Lemerle, J. Ferré, C. Chappert, V. Mathet, T. Giamarchi, and P. Le Doussal, Phys. Rev. Lett. **80**, 849 (1998).
[6] K. Yamada, J.-P. Jamet, Y. Nakatani, A. Mougin, A. Thiaville, T. Ono, and J. Ferré, Appl. Phys. Express **4**, 113001 (2011).
[7] C. Burrowes, N. Vernier, J.-P. Adam, L. Herrera Diez, K. Garcia, I. Barisic, G. Agnus, S. Eimer, J.-V. Kim, T. Devolder, A. Lamperti, R. Mantovan, B. Ockert, E. E. Fullerton, and D. Ravelosona, Appl. Phys. Lett. **103**, 182401 (2013).
[8] M. Voto, L. Lopez-Diaz, and L. Torres, J. Phys. D **49**, 185001 (2016).

[9] Y. Yoshimura, K.-J. Kim, T. Taniguchi, T. Tono, K. Ueda, R. Hiramatsu, T. Moriyama, K. Yamada, Y. Nakatani, and T. Ono, Nat. Phys. **12**, 157 (2015).
[10] O. A. Tretiakov, D. Clarke, G.-W. Chern, Ya. B. Bazaliy, and O. Tchernyshyov, Phys. Rev. Lett. **100**, 127204 (2008).
[11] D. J. Clarke, O. A. Tretiakov, G.-W. Chern, Ya. B. Bazaliy, and O. Tchernyshyov, Phys. Rev. B **78**, 134412 (2008).
[12] D. Bouzidi and H. Suhl, Phys. Rev. Lett. **65**, 2587 (1990).
[13] J. S. Helman, H. B. Braun, J. S. Broz, and W. Baltensperger, Phys. Rev. B **43**, 5908 (1991).
[14] Y. Le Maho, J.-V. Kim, and G. Tatara, Phys. Rev. B **79**, 174404 (2009).
[15] C. Gourdon, L. Thevenard, S. Haghgoo, and A. Cēbers, Phys. Rev. B **88**, 014428 (2013).
[16] A. L. Balk, M. E. Nowakowski, M. J. Wilson, D. W. Rench, P. Schiffer, D. D. Awschalom, and N. Samarth, Phys. Rev. Lett. **107**, 077205 (2011).
[17] A. Fert and P. M. Levy, Phys. Rev. Lett. **44**, 1538 (1980).
[18] A. Fert, Mater. Sci. Forum **59-60**, 439 (1990).
[19] A. Crépieux and C. Lacroix, J. Magn. Magn. Mater. **182**, 341 (1998).
[20] M. Heide, G. Bihlmayer, and S. Blügel, Phys. Rev. B **78**, 140403 (2008).
[21] A. Thiaville, S. Rohart, É. Jué, Vincent Cros, and A. Fert, Europhys. Lett. **100**, 57002 (2012).
[22] G. Chen, T. Ma, A. T. N'Diaye, H. Kwon, C. Won, Y. Wu, A. K. Schmid *et al.*, Nat. Commun. **4**, 2671 (2013).
[23] J.-P. Tetienne, T. Hingant, L. J. Martínez, S. Rohart, A. Thiaville, L. H. Diez, K. Garcia, J.-P. Adam, J.-V. Kim, J.-F. Roch, I. M. Miron, G. Gaudin, L. Vila, B. Ocker, D. Ravelosona, and V. Jacques, Nat. Commun. **6**, 6733 (2015).
[24] M. J. Benitez, A. Hrabec, A. P. Mihai, T. A. Moore, G. Burnell, D. McGrouther, C. H. Marrows, and S. McVitie, Nat. Commun. **6**, 8957 (2015).
[25] I. Gross, L. J. Martínez, J.-P. Tetienne, T. Hingant, J.-F. Roch, K. Garcia, R. Soucaille, J. P. Adam, J.-V. Kim, S. Rohart, A. Thiaville, J. Torrejon, M. Hayashi, and V. Jacques, Phys. Rev. B **94**, 064413 (2016).
[26] S. Pizzini, J. Vogel, S. Rohart, L. D. Buda-Prejbeanu, E. Jué, O. Boulle, I. M. Miron, C. K. Safeer, S. Auffret, G. Gaudin, and A. Thiaville, Phys. Rev. Lett. **113**, 047203 (2014).
[27] Y. P. Kabanov, Y. L. Iunin, V. I. Nikitenko, A. J. Shapiro, R. D. Shull, L. Y. Zhu, and C. L. Chien, IEEE Trans. Magn. **46**, 2220 (2010).
[28] I. Mihai Miron, T. Moore, H. Szambolics, L. D. Buda-Prejbeanu, S. Auffret, B. Rodmacq, S. Pizzini, J. Vogel, M. Bonfim, A. Schuhl, and G. Gaudin, Nat. Mater. **10**, 419 (2011).
[29] S.-G. Je, D.-H. Kim, S.-C. Yoo, B.-C. Min, K.-J. Lee, and S.-B. Choe, Phys. Rev. B **88**, 214401 (2013).
[30] S. Emori, U. Bauer, S.-M. Ahn, E. Martinez, and G. S. D. Beach, Nat. Mater. **12**, 611 (2013).
[31] K.-S. Ryu, L. Thomas, S.-H. Yang, and S. Parkin, Nat. Nanotechnol. **8**, 527 (2013).
[32] A. Hrabec, N. A. Porter, A. Wells, M. J. Benitez, G. Burnell, S. McVitie, D. McGrouther, T. A. Moore, and C. H. Marrows, Phys. Rev. B **90**, 020402 (2014).
[33] J. Torrejon, J. Kim, J. Sinha, S. Mitani, M. Hayashi, M. Yamanouchi, and H. Ohno, Nat. Commun. **5**, 4655 (2014).
[34] R. Lavrijsen, D. M. F. Hartmann, A. van denBrink, Y. Yin, B. Barcones, R. A. Duine, M. A. Verheijen, H. J. M. Swagten, and B. Koopmans, Phys. Rev. B **91**, 104414 (2015).
[35] R. Soucaille, M. Belmeguenai, J. Torrejon, J.-V. Kim, T. Devolder, Y. Roussigné, S.-M. Chérif, A. A. Stashkevich, M. Hayashi, and J.-P. Adam, Phys. Rev. B **94**, 104431 (2016).
[36] É. Jué, A. Thiaville, S. Pizzini, J. Miltat, J. Sampaio, L. D. Buda-Prejbeanu, S. Rohart, J. Vogel, M. Bonfim, O. Boulle, S. Auffret, I. M. Miron, and G. Gaudin, Phys. Rev. B **93**, 014403 (2016).
[37] D. Lau, V. Sundar, J.-G. Zhu, and V. Sokalski, Phys. Rev. B **94**, 060401 (2016).
[38] T. Ha Pham, J. Vogel, J. Sampaio, M. Vaňatka, J.-C. Rojas-Sánchez, M. Bonfim, D. S. Chaves, F. Choueikani, P. Ohresser, E. Otero, A. Thiaville, and S. Pizzini, Europhys. Lett. **113**, 67001 (2016).
[39] F. Garcia-Sanchez, P. Borys, A. Vansteenkiste, J.-V. Kim, and R. L. Stamps, Phys. Rev. B **89**, 224408 (2014).
[40] F. Garcia-Sanchez, P. Borys, R. Soucaille, J.-P. Adam, R. L. Stamps, and J.-V. Kim, Phys. Rev. Lett. **114**, 247206 (2015).
[41] R. W. Damon and J. R. Eshbach, J. Phys. Chem. Solids **19**, 308 (1961).
[42] J. P. Pellegren, D. Lau, and V. Sokalski, Phys. Rev. Lett. **119**, 027203 (2017).
[43] A. N. Bogdanov and U. K. Rößler, Phys. Rev. Lett. **87**, 037203 (2001).
[44] A. Thiaville and Y. Nakatani, in *Spin Dynamics in Confined Magnetic Structures III* (Springer, Heidelberg, 2006), pp. 161–205.
[45] A. L. Balk, K.-W. Kim, D. T. Pierce, M. D. Stiles, J. Unguris, and S. M. Stavis, Phys. Rev. Lett. **119**, 077205 (2017).
[46] O. Boulle, S. Rohart, L. D. Buda-Prejbeanu, E. Jué, I. M. Miron, S. Pizzini, J. Vogel, G. Gaudin, and A. Thiaville, Phys. Rev. Lett. **111**, 217203 (2013).
[47] D.-Y. Kim, D.-H. Kim, and S.-B. Choe, Appl. Phys. Express **9**, 053001 (2016).
[48] H.-B. Braun, J. Kyriakidis, and D. Loss, Phys. Rev. B **56**, 8129 (1997).
[49] J.-V. Kim, in *Solid State Physics*, Vol. 63, edited by R. L. Stamps and R. E. Camley (Academic Press, San Diego, 2012), Chap. 4, pp. 217–294.
[50] H.-B. Braun, Adv. Phys. **61**, 1 (2012).
[51] J. M. Winter, Phys. Rev. **124**, 452 (1961).
[52] H.-B. Braun, Phys. Rev. B **50**, 16485 (1994).
[53] A. Vansteenkiste, J. Leliaert, M. Dvornik, M. Helsen, F. Garcia-Sanchez, and B. Van Waeyenberge, AIP Adv. **4**, 107133 (2014).
[54] S. Rohart and A. Thiaville, Phys. Rev. B **88**, 184422 (2013).
[55] S. Zhang and O. Tchernyshyov, arXiv:1801.07166.
[56] K. Di, V. L. Zhang, H. S. Lim, S. C. Ng, M. H. Kuok, J. Yu, J. Yoon, X. Qiu, and H. Yang, Phys. Rev. Lett. **114**, 047201 (2015).
[57] J.-H. Moon, S.-M. Seo, K.-J. Lee, K.-W. Kim, J. Ryu, H.-W. Lee, R. D. McMichael, and M. D. Stiles, Phys. Rev. B **88**, 184404 (2013).
[58] O. Gladii, M. Haidar, Y. Henry, M. Kostylev, and M. Bailleul, Phys. Rev. B **93**, 054430 (2016).

Correction: A typographical error in the city of third affiliation has been fixed.